International Journal of Nanomedicine

Dovepress
open access to scientific and medical research

Open Access Full Text Article

ORIGINAL RESEARCH

SnO_2-Doped ZnO/Reduced Graphene Oxide Nanocomposites: Synthesis, Characterization, and Improved Anticancer Activity via Oxidative Stress Pathway

This article was published in the following Dove Press journal:
International Journal of Nanomedicine

Maqusood Ahamed[1]
Mohd Javed Akhtar[1]
MA Majeed Khan[1]
Hisham A Alhadlaq[1,2]

[1]King Abdullah Institute for Nanotechnology, King Saud University, Riyadh 11451, Saudi Arabia; [2]Department of Physics and Astronomy, College of Science, King Saud University, Riyadh 11451, Saudi Arabia

International Journal of Nanomedicine downloaded from https://www.dovepress.com/
For personal use only.

Background: Therapeutic selectivity and drug resistance are critical issues in cancer therapy. Currently, zinc oxide nanoparticles (ZnO NPs) hold considerable promise to tackle this problem due to their tunable physicochemical properties. This work was designed to prepare SnO_2-doped ZnO NPs/reduced graphene oxide nanocomposites (SnO_2-ZnO/rGO NCs) with enhanced anticancer activity and better biocompatibility than those of pure ZnO NPs.

Materials and Methods: Pure ZnO NPs, SnO_2-doped ZnO (SnO_2-ZnO) NPs, and SnO_2-ZnO/rGO NCs were prepared via a facile hydrothermal method. Prepared samples were characterized by field emission transmission electron microscopy (FETEM), energy dispersive spectroscopy (EDS), field emission scanning electron microscopy (FESEM), X-ray diffraction (XRD), ultraviolet-visible (UV-VIS) spectrometer, and dynamic light scattering (DLS) techniques. Selectivity and anticancer activity of prepared samples were assessed in human breast cancer (MCF-7) and human normal breast epithelial (MCF10A) cells. Possible mechanisms of anticancer activity of prepared samples were explored through oxidative stress pathway.

Results: XRD spectra of SnO_2-ZnO/rGO NCs confirmed the formation of single-phase of hexagonal wurtzite ZnO. High resolution TEM and SEM mapping showed homogenous distribution of SnO_2 and rGO in ZnO NPs with high quality lattice fringes without any distortion. Band gap energy of SnO_2-ZnO/rGO NCs was lower compared to SnO_2-ZnO NPs and pure ZnO NPs. The SnO_2-ZnO/rGO NCs exhibited significantly higher anticancer activity against MCF-7 cancer cells than those of SnO_2-ZnO NPs and ZnO NPs. The SnO_2-ZnO/rGO NCs induced apoptotic response through the upregulation of caspase-3 gene and depletion of mitochondrial membrane potential. Mechanistic study indicated that SnO_2-ZnO/rGO NCs kill cancer cells through oxidative stress pathway. Moreover, biocompatibility of SnO_2-ZnO/rGO NCs was also higher against normal breast epithelial (MCF10A cells) in comparison to SnO_2-ZnO NPs and ZnO NPs.

Conclusion: SnO_2-ZnO/rGO NCs showed enhanced anticancer activity and better biocompatibility than SnO_2-ZnO NPs and pure ZnO NPs. This work suggested a new approach to improve the selectivity and anticancer activity of ZnO NPs. Studies on antitumor activity of SnO_2-ZnO/rGO NCs in animal models are further warranted.

Keywords: ZnO nanocomposites, improved anticancer activity, better selectivity, reactive oxygen species, caspase-3, breast cancer

Correspondence: Maqusood Ahamed
King Abdullah Institute for Nanotechnology, King Saud University, Riyadh 11451, Saudi Arabia
Email mahamed@ksu.edu.sa

submit your manuscript | www.dovepress.com
DovePress
http://doi.org/10.2147/IJN.S285392

© 2021 Ahamed et al. This work is published and licensed by Dove Medical Press Limited. The full terms of this license are available at https://www.dovepress.com/terms.php and incorporate the Creative Commons Attribution – Non Commercial (unported, v3.0) License (http://creativecommons.org/licenses/by-nc/3.0/). By accessing the work you hereby accept the Terms. Non-commercial uses of the work are permitted without any further permission from Dove Medical Press Limited, provided the work is properly attributed. For permission for commercial use of this work, please see paragraphs 4.2 and 5 of our Terms (https://www.dovepress.com/terms.php).

Introduction

According to a World Health Organization (WHO) report, cancer is the second leading cause of death worldwide.[1] It has also been estimated that the total number of cancer cases will be doubled by year 2030 from 12.4 million new cases reported in 2008.[2] In spite of the incredible effort to treat cancer, a lot needs to be done in cancer therapy. Recent cancer chemotherapies often fail to provide a complete anticancer response due to the development of drug resistance or their inability to efficiently differentiate between cancerous and noncancerous cells.[3] This indiscriminate action normally leads to systemic toxicity in the human body.

Cancer nanotechnology can play a crucial role in the diagnosis and treatment of cancer to improve human health.[4] A growing number of studies demonstrated that certain types of metal oxide nanoparticles (NPs) can selectively kill cancer cells with low toxicity to their normal counterparts.[5–8] Particularly, ZnO NPs showed great promise for cancer therapy. Due to unique physiochemical characteristics ZnO NPs have shown inherent selective toxicity against cancer cells while posing minimum effects to the normal cells.[9–11] ZnO NPs induce apoptosis in cancer cells through the generation of ROS and depletion of mitochondrial membrane potential (MMP)[12,13] Manipulation in intracellular ROS generation is a probable way to irreversibly damage cancerous cells selectively without applying much harm to normal cells. The ROS-generating potential of ZnO NPs is associated with its optical properties.[14] Optical behavior of ZnO NPs can be tuned by several methods including metal ion doping and synthesis of ZnO-based nanocomposites.[14,15]

Alternatively, studies reported some degree of toxicity of ZnO NPs in a wide range of organisms such as bacterial, microalgae, yeast, protozoa, zebrafish, and mice.[16–20] Hence, there is an urgent need to tailor ZnO NPs with improved selectivity and anticancer activity.[21] Semiconductor tin oxide (SnO_2) and reduced graphene oxide (rGO) have shown great potential for biomedical applications.[5,22] SnO_2 and rGO can also be applied to tune physicochemical properties of metal oxide NPs including ZnO.[23,24]

Keeping the above points in mind, we prepared SnO_2-doped ZnO NPs/reduced graphene oxide nanocomposites (SnO_2-ZnO/rGO NCs) with improved anticancer potential and higher biocompatibility as compared to pure ZnO NPs. Pure ZnO NPs, SnO_2-ZnO NPs, and SnO_2-ZnO /rGO NCs were prepared through a facile hydrothermal method. Prepared samples were characterized by field emission electron microscopy (FETEM), energy dispersive spectroscopy (EDS), field emission scanning electron microscopy (FESEM), X-ray diffraction (XRD), ultraviolet-visible (UV-VIS) spectrometer, and dynamic light scattering (DLS) techniques. Anticancer activity of pure ZnO NPs, SnO_2-ZnO NPs, and SnO_2-ZnO/rGO NCs was examined in human breast cancer (MCF-7) cells. Possible mechanism of anticancer potentials of SnO_2-ZnO/rGO NCs was delineated through ROS pathway. Biocompatibility of prepared samples were investigated in human normal breast epithelial (MCF10A) cells. Breast cancer cell lines were chosen in the present study because female breast cancer is the most commonly diagnosed cancer and the third leading cause of cancer death globally after colorectal and lung cancer.[2]

Materials and Methods

Synthesis of ZnO NPs, SnO_2-ZnO NPs, and SnO_2-doped-ZnO/rGO NCs

GO was prepared from pure graphite powder (<150 μm, 99.99% trace metals basis) (Millipore-Sigma, St Louis, MO, USA) applying modified Hummers' protocol.[25] The SnO_2-doped ZnO/rGO nanocomposite were synthesized through a facile hydrothermal method. Firstly, 0.02 g of GO was dispersed into 20 mL of ethanol (C_2H_5OH) (Millipore-Sigma) and sonicated for three hours in an ultrasonic bath to get uniform GO suspension. Zinc acetate dihydrate ($Zn(CH_3COO)_2.2H_2O$) (99.999% trace metals basis, Millipore-Sigma) (2 mM), tin (II) chloride dihydrate ($SnCl_2.2H_2O$) (≥99.995% trace metals basis, Millipore-Sigma) (0.1 mM), and polyethylene glycol (PEG) (Millipore-Sigma) (0.2 g) were mixed in 20 mL distilled water under continuous stirring for one hour at room temperature to get homogenous solution. Then, GO suspension was mixed with homogenous solution and stirred for one hour, and pH of solution was maintained at 9 by adding aqueous ammonia solution. Then, solution transferred into a 50 mL autoclave and heated at 160°C for 12 h. Finally, the grey precipitates were washed and dried at 50°C for 12 h to get SnO_2-ZnO/rGO nanocomposites. SnO_2-doped ZnO NPs was prepared in similar procedure without adding GO, and pure ZnO NPs was synthesized without addition of tin chloride and GO during hydrothermal process. A schematic diagram of SnO_2-ZnO/rGO NCs synthesis is given in Figure 1.

Characterization

Absorption spectra of prepared samples were recorded at the wavelength of 300–900 nm with a resolution of 0.5 nm (Shimadzu UV-1800 spectrometer, Reinach BL, Switzerland). Crystallinity and phase-purity were analyzed at powder X-ray diffraction (PXRD) (PanAnalytic X'Pert Pro, Malvern Instruments, UK) with Cu-Kα radiation (λ=0.15405 nm, at 45 kV and 40 mA). Structural characterization was further assessed through FETEM (JEM-2100F, JEOL, Inc., Tokyo, Japan). Elemental analysis was done by energy dispersive X-ray spectroscopy (EDS). Mapping of elemental distribution of SnO_2-ZnO /rGO NCs was further done through FESEM (JSM-7600F, JEOL, Inc.). Hydrodynamic size and zeta potential in distilled water and culture medium were determined by DLS (ZetaSizer, Nano-HT, Malvern Instruments).

Cell Culture and Exposure Procedure

MCF-7 cells (ATCC HTB-22, ATCC, Virginia, USA) were cultured in DMEM (Invitrogen, Carlsbad, CA, USA) with 10% FBS and antibiotics (100 µg/mL streptomycin+100 U/mL penicillin). MCF10A (ATCC CRL-10317) cells were grown in mammary epithelial cell growth basal medium (MEBM) (Lonza Group Ltd, Basel, Switzerland) supplemented with mammary epithelial cell growth medium (MEGM) kit (Lonza Group Ltd) and 100 ng/mL cholera toxin. Cells

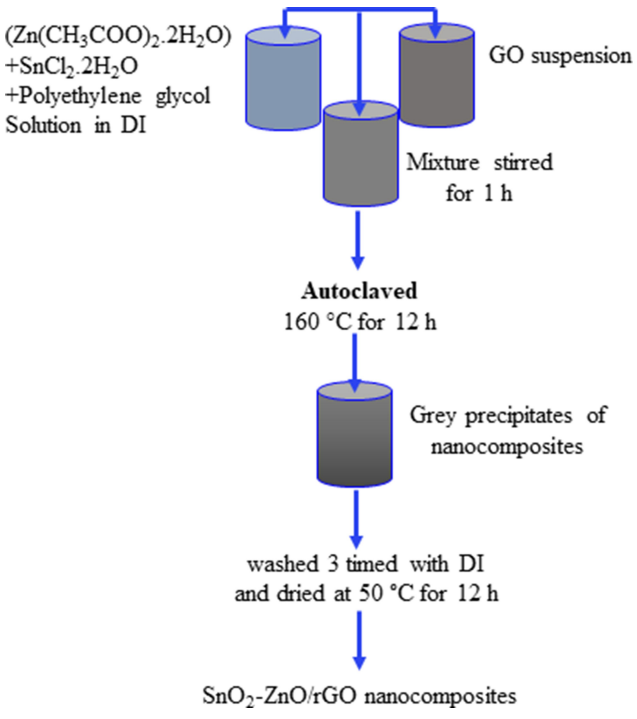

Figure 1 A schematic diagram of SnO_2-ZnO/rGO NCs synthesis.

were maintained in a humidified incubator under control conditions (37°C and 5% CO_2). First, we exposed the cells with a range of concentrations (0–200 µg/mL) of ZnO NPs, SnO_2-ZnO NPs, and SnO_2-ZnO/rGO NCs for 24 h for cell viability assay. On the basis of cell viability results, we have chosen three moderate concentrations (10, 25, and 50 µg/mL) of these samples for further experiments. For microscopic study we have chosen one concentration (50 µg/mL) of prepared samples. In some experiments, cells were exposed to ZnO NPs, SnO_2-ZnO NPs, and SnO_2-ZnO/rGO NCs with or without N-acetyl-cysteine (NAC) (2 mM) (Millipore-Sigma). Briefly, NPs/NCs were suspended in culture medium (DMEM+10% FBS) and diluted to desired concentration (0–200 µg/mL). Different dilutions of NPs were further sonicated utilizing sonicator bath at room temperature for 10 min at 40 W to avoid agglomeration of NPs/NCs before exposure to cells. Cells without NPs/NCs served as control in each experiment.

Biochemical Assays

Cell viability was determined through MTT[26] and NRU[27] assays with some specific changes.[28] Morphology of treated and control cells was grabbed through phase-contrast inverted microscope (Leica Microsystems, GmbH, Germany). Expression level of mRNA of caspase-3 gene (*CASP3*) was determined through real-time PCR (ABI PRISM, 7900HT Sequence Detection System) (Applied Biosystems, Foster City, CA, USA) according to the procedures described earlier.[28,29] Colorimetric assay of caspase-3 enzyme was performed using BioVision kit (Milpitas, CA, USA). MMP was assayed using rhodamine-123 probe (Rh-123) (Millipore-Sigma).[30] MMP level was quantitatively assayed through a microplate reader (Synergy-HT, BioTek Winooski, VT, USA) and intracellular images were grabbed using a DMi8 fluorescent microscope (Leica Microsystems). Intracellular level of ROS was assayed using 2′-7′-dichlorodihydrofluorescein diacetate (H_2DCFDA, Millipore-Sigma) probe.[8] ROS level was also determined both quantitatively (Microplate reader, Synergy-HT, BioTek) and qualitatively (DMi8 fluorescent microscope, Leica Microsystems). Fluorometric assay of intracellular hydrogen peroxide (H_2O_2) was done applying a commercial kit (MAK164 green fluorescence, Millipore-Sigma). Glutathione (GSH) level was quantified using Ellman's method.[31] Malondialdehyde (MDA), one of the end products of lipid peroxidation was estimated using procedures of Ohkawa et al.[32] Glutathione peroxidase (GPx) enzyme activity was assayed applying methods of Rotruck et al.[33] Procedures of Sinha were utilized to assay the

catalase (CAT) enzyme activity[34] Colorimetric assay of superoxide dismutase (SOD) enzyme was done using kit from Cayman Chemical Company (Michigan, OH, USA). Protein content was quantified using Bradford's protocol.[35] Brief description of each biochemical procedure with necessary steps is provided in supplementary information.

Statistical Analysis

One-way ANOVA followed by Dunnett's multiple comparison tests were applied for analysis of results. The $p<0.05$ was assigned as statistically significant.

Results and Discussion

Morphological and Microstructural Study

Morphology, particle size, and crystal structure of ZnO NPs, SnO_2-ZnO NPs, and SnO_2-ZnO/rGO NCs were determined by FETEM. Figure 2A showed that ZnO NPs were almost spherical shaped with size of 14 nm. It was noticed that the shape of nanoparticles remains same, but the size of NPs increases after SnO_2 doping (19 nm) (Figure 2B) and rGO integration (29 nm) (Figure 2C). Increment of NP size after doping and rGO incorporation was also reported by other studies.[15] Figure 2D–F showed the HRTEM of ZnO NPs, SnO_2-ZnO NPs, and SnO_2-ZnO /rGO NCs, respectively. These images depict the presence of ZnO, SnO_2 and rGO with high quality lattice fringes without any distortion. The calculated interplanar spacing of adjacent lattice fringes of ZnO NPs, SnO_2-ZnO NPs, and SnO_2-ZnO/rGO NCs were 0.345 nm, 0.342 nm, and 0.340 nm that correspond to the (101) plane of hexagonal wurtzite structure of ZnO.[36] The lattice fringes of SnO_2 were 0.334 nm and 0.338 nm corresponding to the (110) planes of tetragonal phase of SnO_2.[23] The lattice fringes were in agreement with XRD spectra. TEM images were also suggested all grown particles were highly crystalline that confirm the incorporation of SnO_2 and rGO into the crystalline matrix of ZnO without creating lattice defects. EDS spectra of prepared SnO_2-ZnO/rGO NCs indicated the stoichiometric presence of Zn, Sn, O, and C without any impurities (Figure 3). The Cu peak came from copper grid of TEM. The SEM mapping of elemental distribution of SnO_2-ZnO/rGO NCs showed uniform distribution of SnO_2 and rGO in ZnO NPs (Figure 4).

Crystal structure, phase purity, and size of ZnO NPs, SnO_2-ZnO NPs, and SnO_2-ZnO/rGO NCs were also analyzed by XRD technique. The XRD spectra of all samples were presented in Figure 5A. The indexing of diffraction peaks represents the formation of single-phase hexagonal wurtzite ZnO according to JCPDS card number 36–1451. No clear diffraction peak of SnO_2 indicated that homogeneous doping of SnO_2 throughout the ZnO lattice and ionic radii of Zn (0.74°A) and Sn (0.71°A) are almost same.[37]

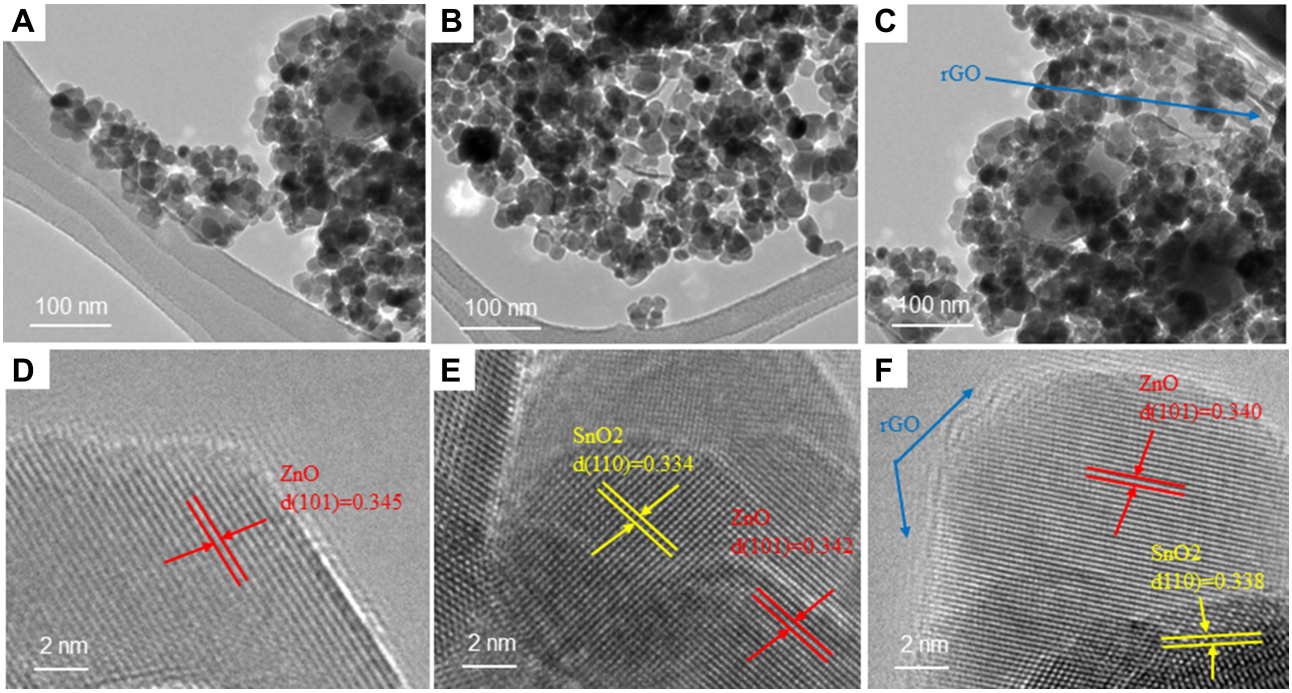

Figure 2 (A–C) Low resolution TEM images and **(D–F)** high resolution TEM images of ZnO NPs, SnO_2-ZnO NPs, and SnO_2-ZnO/rGO NCs. Arrows represent rGO.

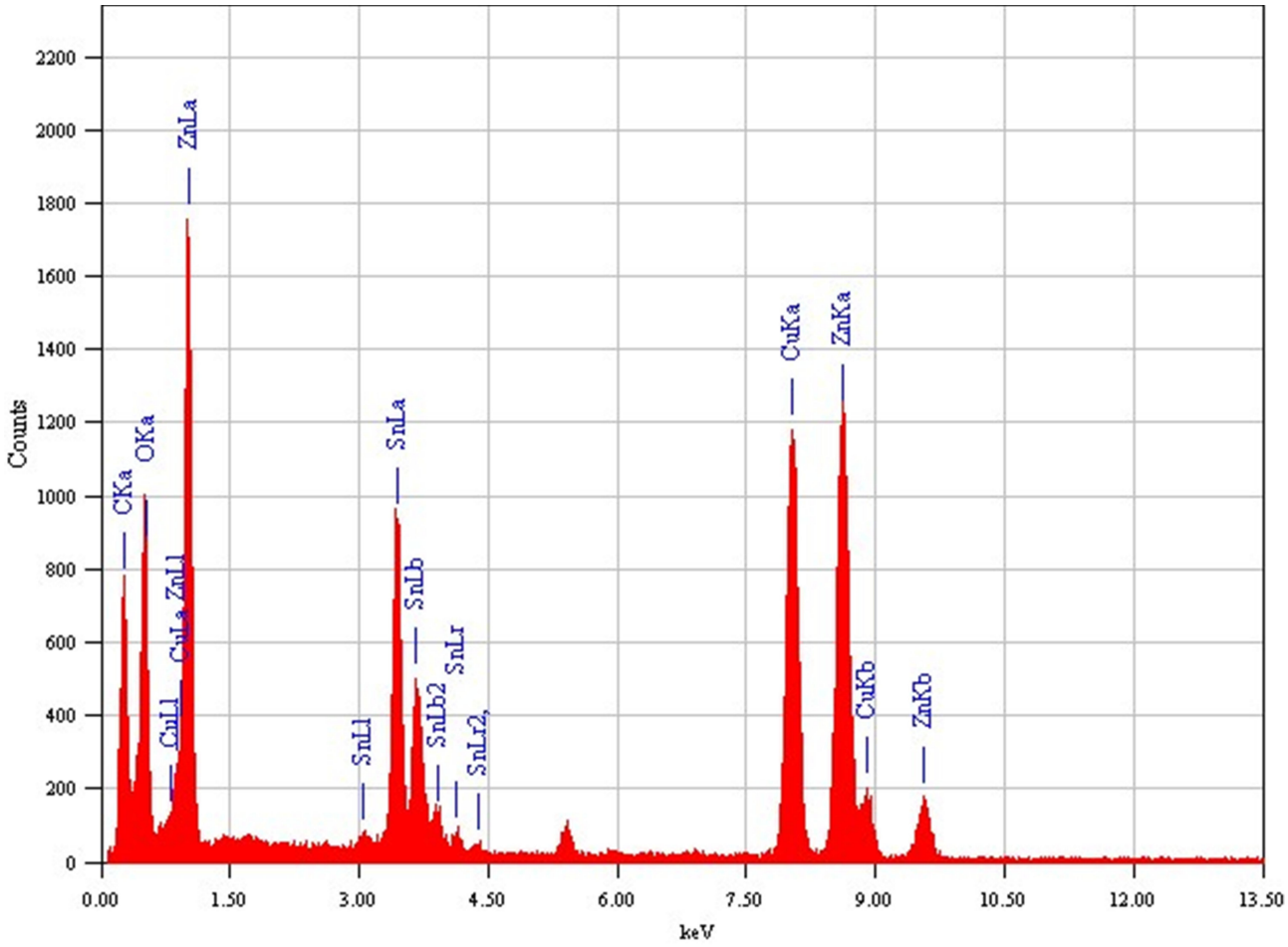

Figure 3 Elemental composition of SnO_2-ZnO/rGO NCs assessed through EDS.

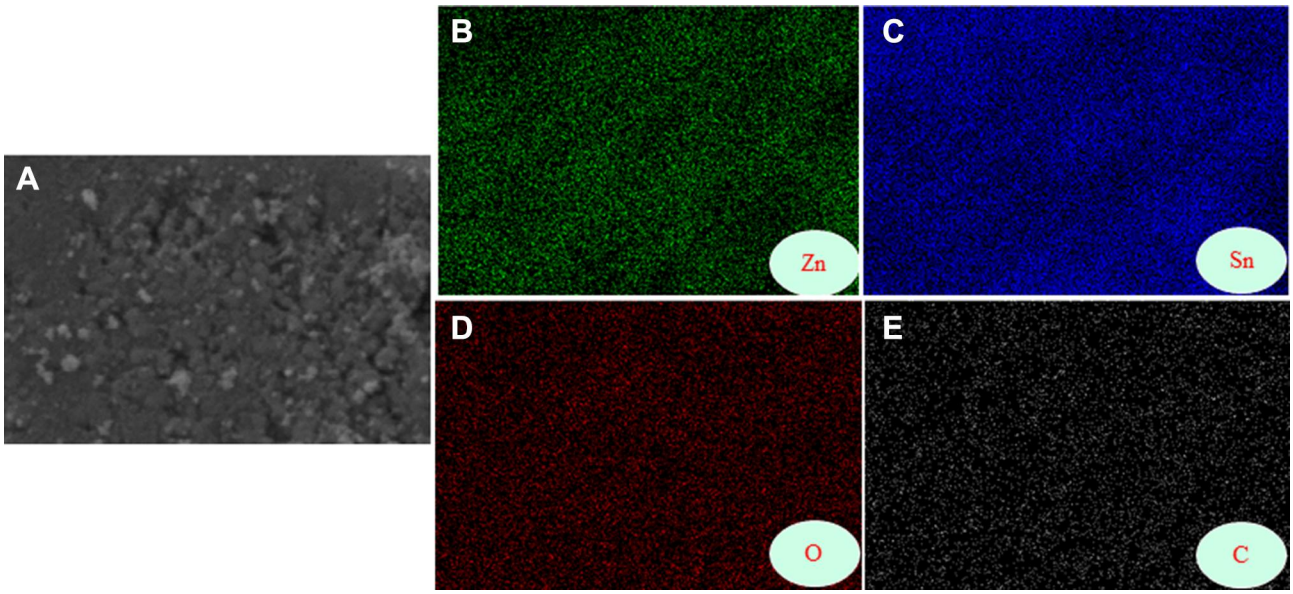

Figure 4 SEM elemental mapping of SnO_2-ZnO/rGO NCs. (**A**) SEM image. (**B**) Zinc. (**C**) Tin. (**D**) Oxygen. (**E**) Carbon mapping.

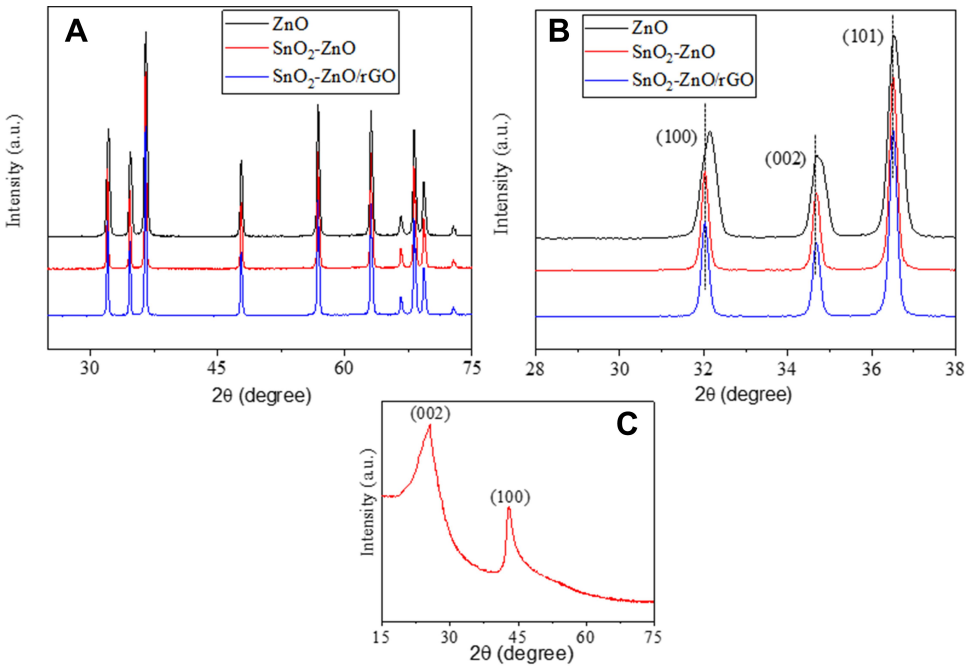

Figure 5 (**A**) XRD spectra of ZnO NPs, SnO_2-ZnO NPs, and SnO_2-ZnO/rGO NCs. (**B**) XRD spectra of same samples in the diffraction region of 28–38. (**C**) XRD spectra of rGO.

Absence of diffraction peak of rGO in XRD spectra of SnO_2-ZnO/rGO NCs also indicate the uniform distribution of SnO_2-ZnO NPs inhibited the restacking of rGO sheets.[38] Besides, XRD spectra show narrow and sharp diffraction peaks depicting excellent crystallinity of prepared samples. Crystallite size of synthesized samples were determined corresponding to highest intensity peak (101) by Scherrer's formula and provided in Table 1. Results showed that crystallite size increases from 15 nm to 31 nm after SnO_2 doping and rGO integration, which was well matched with to size calculated from TEM. We further noticed slight shifting of XRD peaks toward a lower value as compared to pure ZnO (Figure 5B). This shifting also indicates successful integration of SnO_2 and rGO into ZnO NPs. Figure 5C represent XRD spectra of prepared rGO, which shows intense reflection planes (002) and (100).[24]

Table 1 Structural and Optical Properties

Compositions	TEM Size (nm)	XRD size	Optical Band Gap (eV)
ZnO	14.2	15.5	3.30
SnO_2-ZnO	19.4	20.3	3.25
SnO_2-ZnO /rGO	29.8	31.2	3.18

Optical Study

Optical properties of all prepared samples were examined through optical absorption study. Absorption spectra of ZnO NPs, SnO_2-ZnO NPs, and SnO_2-ZnO/rGO NCs, indicates SnO_2 doping and rGO integration shifted the absorption edge of ZnO toward higher wavelength (Figure 6A). The band gap energy (Eg) for ZnO NPs, SnO_2-ZnO NPs, and SnO_2-ZnO/rGO NCs were determined by Tauc's formula.[36]

$$\alpha h\nu = A(h\nu\text{-}Eg)^{1/2}$$

where hν is the photon energy and A is the constant that does not depend on photon energy. The band gap energy (Eg) was determined by the extrapolation of linear portion of $(\alpha h\nu)^2$ vs hν curve to photon energy (hν) axis corresponding to α=0 (Figure 6B). The band gap values are provided in Table 1, which represent a decrement in band gap of ZnO NPs after SnO_2 doping and rGO integration (3.30 eV-3.18 eV). It is reported that band gap energy of ZnO NPs could be tuned by doping metals oxides and/or integration of other semiconducting materials. Our results are in agreement with previous studies.[39–41] Band gap tuning of ZnO NPs might be useful in cancer therapy. Tuning of band gap of semiconductor NPs might increase the threshold of ROS generation and oxidative stress in cancer cells through the generation of higher holes (h^+) and electrons (e^-) on the surface of NPs.[8,42]

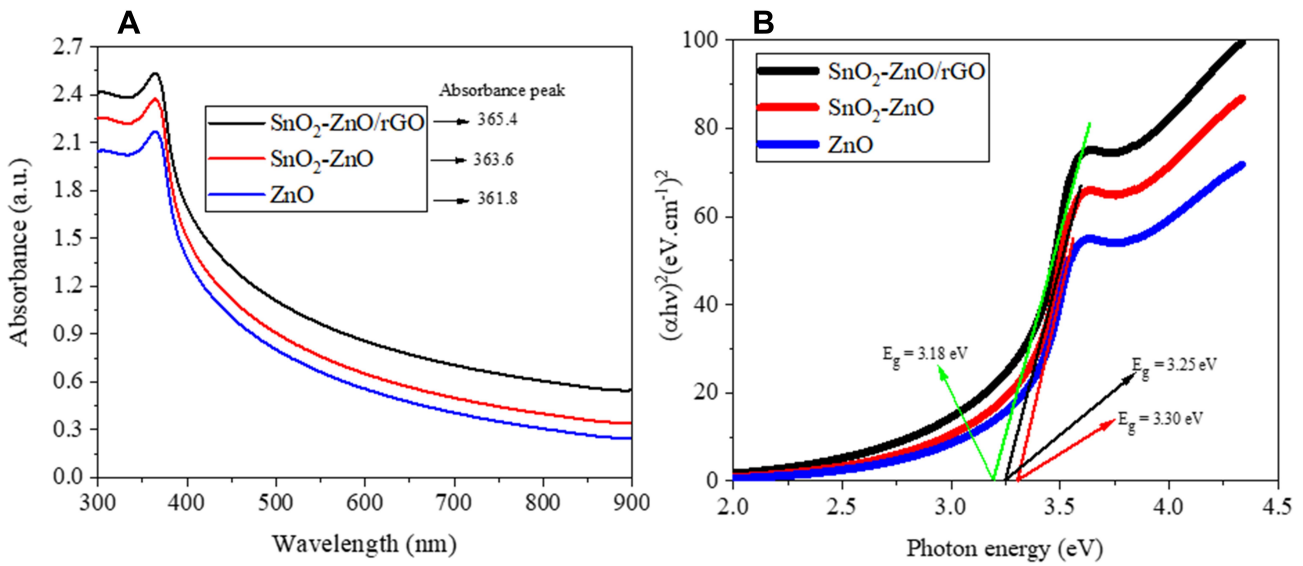

Figure 6 (**A**) optical absorption spectra of ZnO NPs, SnO_2-ZnO NPs, and SnO_2-ZnO/rGO NCs. (**B**) Tauc's plot $(\alpha h\nu)^2$ vs (hν) of the same samples.

Dynamic Light Scattering Study

It is important to assess the colloidal stability and surface charge of NPs in physiological media to understand the interaction of NPs with biological systems. DLS was applied to examine the hydrodynamic size and zeta potential of ZnO NPs, SnO_2-ZnO NPs, and SnO_2-ZnO/rGO NCs in distilled water and culture medium (Table 2). Hydrodynamic size of these samples in distilled water and culture medium were in the range of 55 nm to 96 nm, which were around three-to-five times higher than those of powder size calculated from TEM and XRD. Higher hydrodynamic size could be due to the agglomeration of particles in aqueous suspension and also reported in earlier studies.[5,8,43] Zeta potential data showed that particles surface charge were ranging from 25–30 eV in distilled water and culture medium (DMEM +FBS). Zeta potential data suggested that colloidal suspension of prepared NPs and NCs were fairly stable. The higher value of zeta potential (positive or negative), the greater is the colloidal stability of nanoscale materials.[44,45] Positive surface charge of prepared NPs and NCs under physiological medium provides favorable condition for their interaction with cancerous cells, which frequently carry negative surface charge.[45]

Cytotoxicity

Anticancer potential of ZnO NPs can be further improved by tuning of its physicochemical properties.[3] In this study, we tried to enhance the cytotoxic potential of ZnO NPs against cancer cells through SnO_2 doping and integration of rGO to prepare ZnO nanocomposites. Cytotoxicity of ZnO NPs, SnO_2-ZnO NPs, and SnO_2-ZnO/rGO NCs in breast cancer MCF-7 cells was assessed through MTT, NRU, and morphological examination. MCF-7 cells were exposed to different concentrations (0–200 µg/mL) of these samples for 24 h. MTT results demonstrated that all three samples were found to reduce cell viability in a dose-dependent manner in the concentration range of 10–200 µg/mL (Figure 7A). Furthermore, we observed that cytotoxicity of SnO_2-ZnO/rGO NCs were significantly higher in comparison to pure ZnO NPs. MTT cell viability data were utilized to calculate the IC_{50s} of prepared samples in MCF-7 cells. IC_{50s} for ZnO NPs, SnO_2-ZnO NPs,

Table 2 Dynamic Light Scattering Characterization

Compositions	Hydrodynamic Size (nm)		Zeta Potential (mV)	
	Distilled Water	Culture Medium	Distilled Water	Culture Medium
ZnO	55.3±5.4	57.8±4.6	26.3±1.4	25.7±2.3
SnO_2-ZnO	69.6±4.3	77.6±5.1	27.6±1.7	26.5±1.6
SnO_2-ZnO/rGO	81.4±2.7	96.4±4.4	30.3±2.1	29.3±1.9

and SnO_2-ZnO/rGO NCs were 54.61, 38.73, and 27.86 µg/mL, respectively (Figure S1 and Table S1 of supplementary information). NRU data on cell viability was according to MTT results (Figure 7B). Figure 7C demonstrated that cell morphology after exposure to 50 µg/mL of ZnO, SnO_2-ZnO, and SnO_2-ZnO/rGO for 24 h. These images suggested that a significant number of cell death occurs (rounded morphology and low cell density) after exposure to ZnO NPs, SnO_2-ZnO NPs, and SnO_2-ZnO/rGO NCs compared to controls. Similar to cell viability results, cell death induced by SnO_2-ZnO /rGO NCs were greater than those of SnO_2-ZnO NPs and pure ZnO NPs. Cytotoxic potential of ZnO NPs against different types of cancer cell lines has also been reported by other investigators.[46–48] For example, a recent study reported anticancer activity of ZnO NPs against human small-cell lung cancer in an orthotopic mouse model.[10]

Apoptosis

Apoptosis (a form of programmed cell death) might be stimulated by various internal or external factors such as injury, stress, starvation, and known apoptotic agents.[49] ZnO NPs induce apoptosis in cancer cells through caspase-activation and MMP depletion.[12,13] Caspase-3 is a protease that is present in mitochondria and critically involved in apoptotic pathway.[50] Apoptotic response of prepared samples was determined by measuring the regulation of caspase-3 gene and MMP level in MCF-7 cells. Figure 8A showed that in comparison to control, ZnO NPs, SnO_2-ZnO NPs, and SnO_2-ZnO/rGO NCs upregulated the mRNA expression level of the *CASP3* gene in a dose-dependent manner (10–50 µg/mL). To confirm the mRNA data, we further examined the activity of caspase-3 enzyme (protein level). Results showed that activity of caspase-3 enzyme was dose-dependently higher in ZnO NPs, SnO_2-ZnO NPs, and

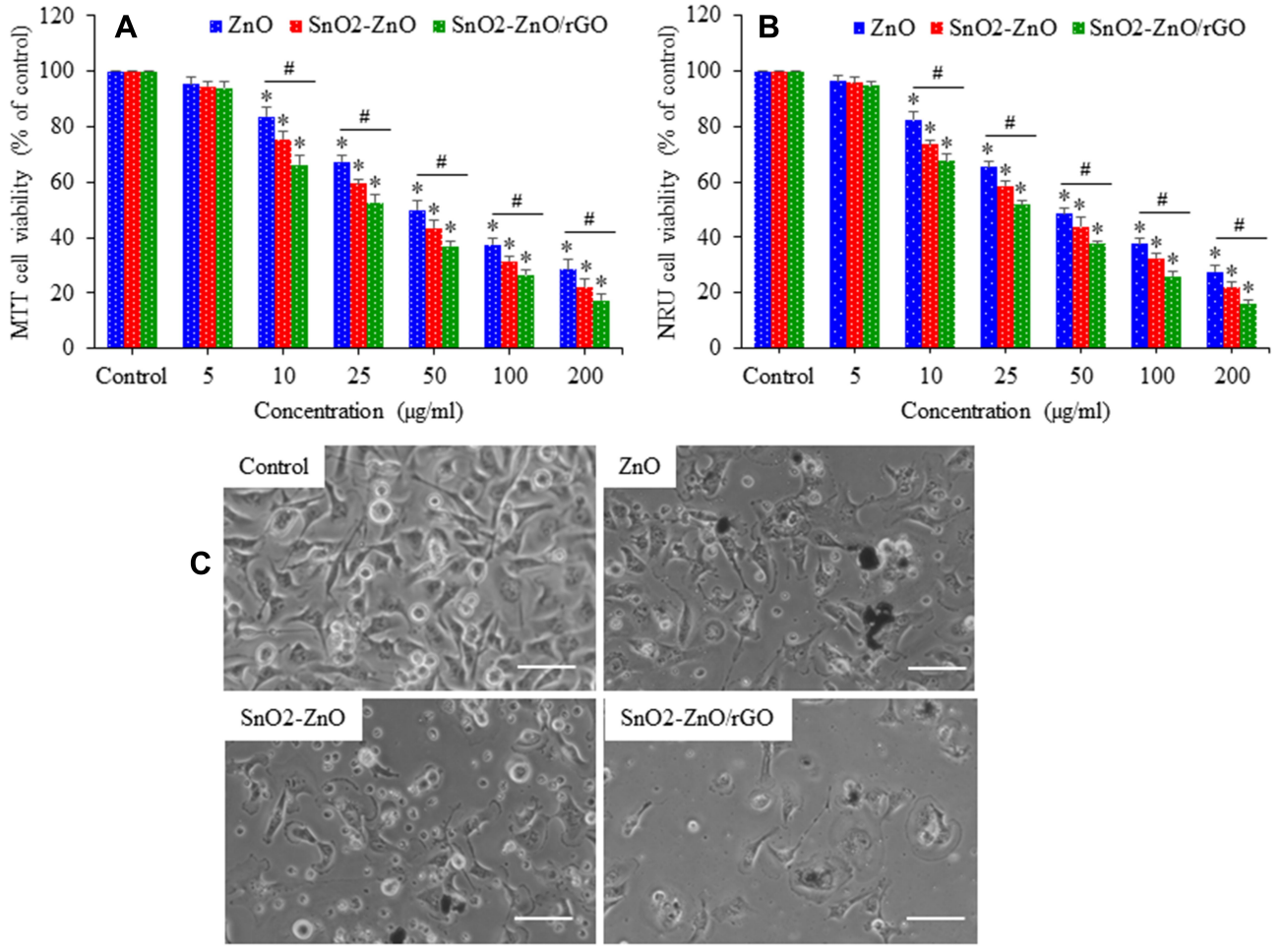

Figure 7 Cytotoxic potential of ZnO NPs, SnO_2-ZnO NPs, and SnO_2-ZnO/rGO NCs in MCF-7 cells. Cells were treated for 24 h to different concentration of these samples (0–200 µg/mL). (**A**) MTT cell viability. (**B**) NRU cell viability. (**C**) Cell morphology after exposure to 50 µg/mL of ZnO NPs, SnO_2-ZnO NPs, and SnO_2-ZnO/rGO NCs for 24 h. (Scale bar presents 50 µm.) Data represented as mean ±SD of five independent experiments (n=5). $^*p<0.05$ control vs treated groups and $^{\#}p<0.05$ pure ZnO NPs vs SnO_2-ZnO/rGO NCs.

SnO_2-ZnO/rGO NCs treated groups compared to control group (Figure 8B). Moreover, effect of SnO_2-ZnO/rGO NCs on activation of the caspase-3 gene was significantly higher than those of pure ZnO NPs.

MMP level of cells is compromised under stressful condition and is an excellent indicator of apoptosis.[51] Figure 8C showed that dose-dependent reduction in MMP level after exposure to ZnO NPs, SnO_2-ZnO NPs, and SnO_2-ZnO/rGO NCs. Fluorescent microscopy data also indicated that brightness of Rh-123 probe decreases (indicator of MMP loss) in all three samples ZnO NPs, SnO_2-ZnO NPs, and SnO_2-ZnO/rGO NCs compared to control (Figure 8D). Similarly, MMP loss caused by SnO_2-ZnO/rGO NCs was significantly higher in comparison to pure ZnO NPs. Apoptosis mediated anticancer activity of ZnO NPs was also reported by other investigators. Duan et al observed the anticancer activity of ZnO NPs in human melanoma (A375) cells was mediated through MMP depletion and caspase activation.[52] Another recent report also suggested that ZnO NPs induced caspase-dependent apoptosis in gingival squamous cell carcinoma cells mediated through the mitochondrial pathway.[53]

Oxidative Stress

Intracellular ROS generation and oxidative stress have been suggested as a possible mechanism to eliminate cancer cells.[54] Recent studies indicated that ZnO NPs destroy cancer cells through ROS generation.[14,55] Oxidative stress generating potential of ZnO NPs, SnO_2-ZnO NPs, and SnO_2-ZnO/rGO NCs in MCF-7 cells were explored through measuring several markers of pro-oxidants and antioxidants. Figure 9A depicted that all three samples induce ROS generation dose-dependently. Fluorescent microscopic images also suggested

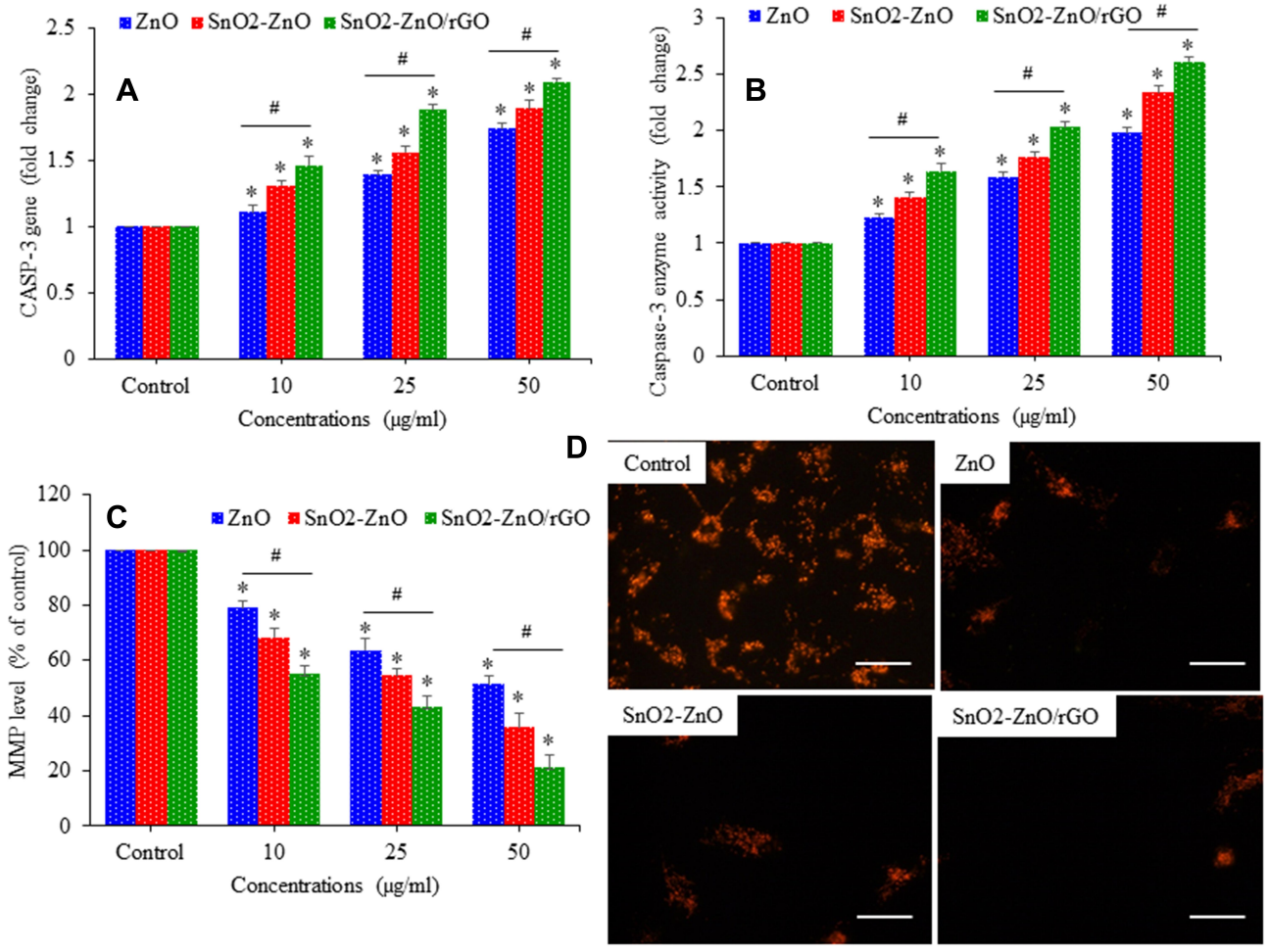

Figure 8 Apoptotic potential of ZnO NPs, SnO_2-ZnO NPs, and SnO_2-ZnO/rGO NCs in MCF-7 cells. Cells were treated for 24 h to different concentration of these samples (10–50 µg/mL). (**A**) mRNA expression level of *CASP3* gene. (**B**) Activity of caspase-3 enzyme. (**C**) Quantitative data MMP. (**D**) Fluorescent cellular images of Rh-123 (MMP indicator) probe after exposure to 50 µg/mL of same samples for 24 h. (Scale bar presents 50 µm.) Data represented as mean ±SD of five independent experiments (n=5). $^{*}p<0.05$ control vs treated groups and $^{\#}p<0.05$ pure ZnO NPs vs SnO_2-ZnO/rGO NCs.

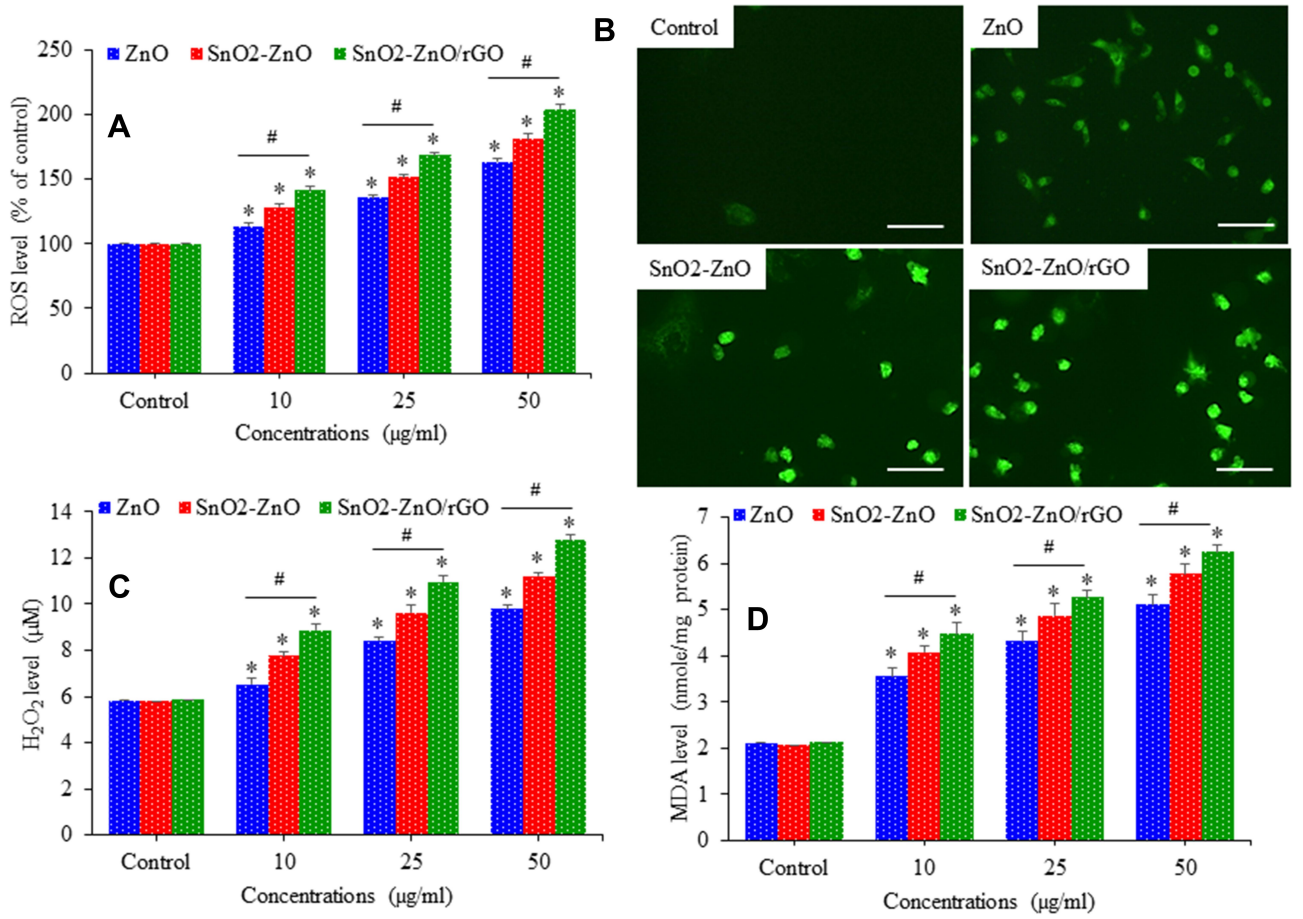

Figure 9 Pro-oxidants generating potential of ZnO NPs, SnO_2-ZnO NPs, and SnO_2-ZnO/rGO NCs in MCF-7 cells. Cells were treated for 24 h to different concentration of these samples (10–50 µg/mL). (**A**) Quantitative data ROS level. (**B**) Fluorescent cellular images of DCF (ROS indicator) probe after exposure to 50 µg/mL of same samples for 24 h. (Scale bar presents 50 µm.) (**C**) Quantitative analysis of intracellular H_2O_2 level (**D**) MDA level. Data represented as mean ±SD of five independent experiments (n=5). *p<0.05 control vs treated groups and $^{\#}p$<0.05 pure ZnO NPs vs SnO_2-ZnO/rGO NCs.

that brightness of DCF probe (indicator of ROS generation) were higher in ZnO NPs, SnO_2-ZnO NPs, and SnO_2-ZnO /rGO NCs treated cells than those of control cells (Figure 9B). Intracellular H_2O_2 level (Figure 9C) and MDA level (Figure 9D) were also significantly higher in ZnO NPs, SnO_2-ZnO NPs, and SnO_2-ZnO/rGO NCs treated cells as compared to controls (p<0.05). Importantly, pro-oxidants generating potential of SnO_2-ZnO/rGO NCs were significantly higher in comparison to pure ZnO NPs.

Cell possesses antioxidant defense systems to get rid of ROS by inducing antioxidant molecule GSH along with several antioxidant enzymes.[56] GSH scavenge ROS and free radicals to protect cells from oxidative damage.[57] Main antioxidant enzymes are GPx, SOD, and CAT. GPx is mainly responsible for removal of hydroperoxides, hence, it may protect membranes, lipids, and proteins from oxidation. SOD provides a first line of defense by converting highly reactive superoxide anion ($O_2^{\bullet-}$) into H_2O_2. CAT further breaks H_2O_2 into water and molecular oxygen.[58] Antioxidant defense potential of MCF-7 cells was assessed following exposure for 24 h to ZnO NPs, SnO_2-ZnO NPs, and SnO_2-ZnO/rGO NCs. (Figure 10A–D) showed that all three samples reduced the GSH level and decreased the activity of several antioxidant enzymes (GPx, SOD, and CAT) in a dose-dependent manner. Again, effects of SnO_2-ZnO/rGO NCs on antioxidant markers were significantly higher than those of pure ZnO NPs.

Possible Mechanism of Anticancer Activity

Higher ROS production that surpasses the antioxidant defense capacity of the cells causes oxidative stress that induces oxidative damage of cellular components such DNA, lipid, and proteins.[9] Recent studies indicated that ROS generation induces enzyme deactivation, lipid peroxidation, and membrane damage, which are the core mechanisms accountable for anticancer activity of ZnO

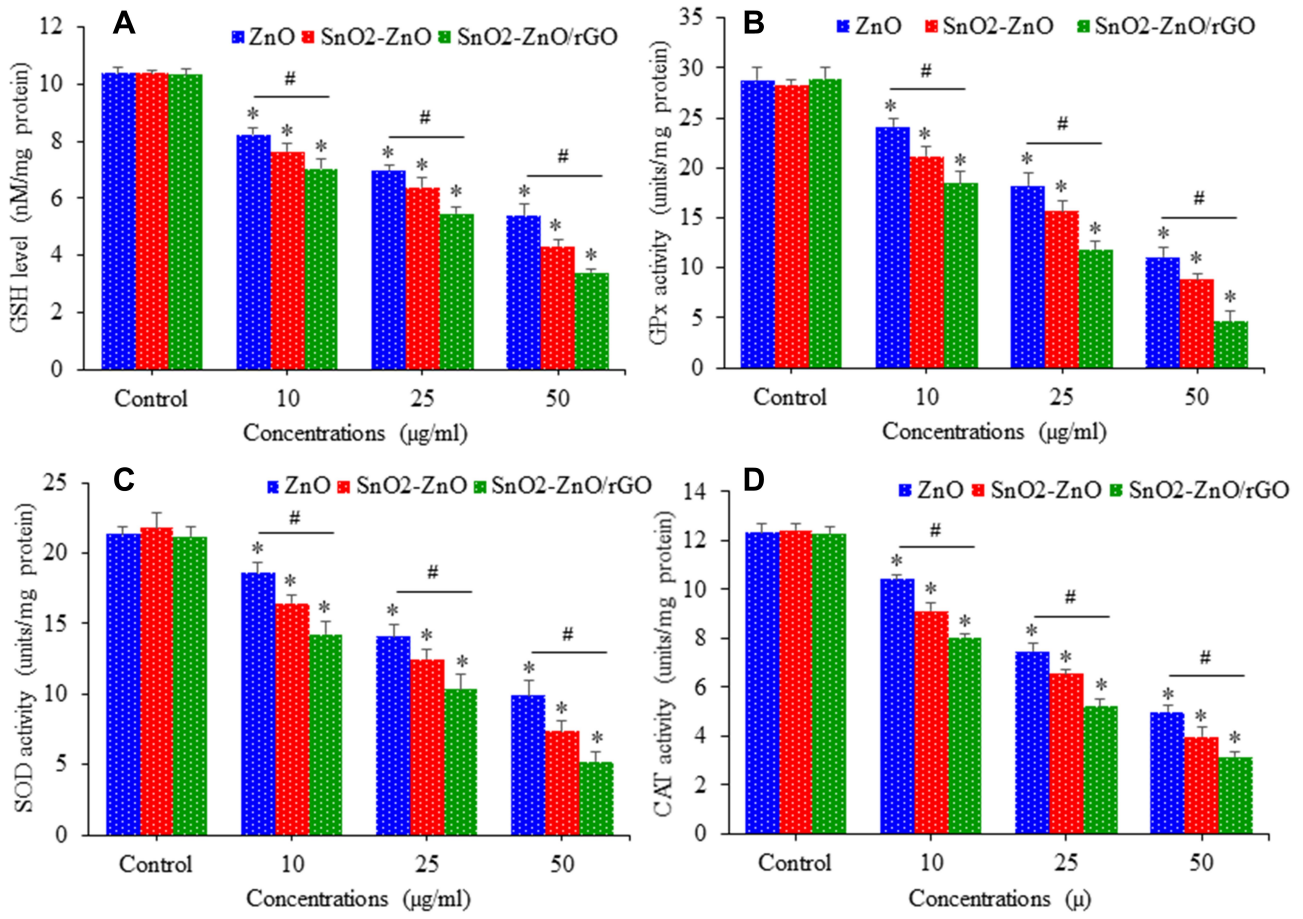

Figure 10 Antioxidants depleting potential of ZnO NPs, SnO_2-ZnO NPs, and SnO_2-ZnO/rGO NCs. In MCF-7 cells. Cells were treated for 24 h to different concentration of these samples (10–50 µg/mL). (**A**) GSH level. (**B**) GPx activity. (**C**) SOD activity. (**D**) CAT activity. Data represented as mean ±SD of five independent experiments (n=5). *p<0.05 control vs treated groups and #p<0.05 pure ZnO NPs vs SnO_2-ZnO/rGO NCs.

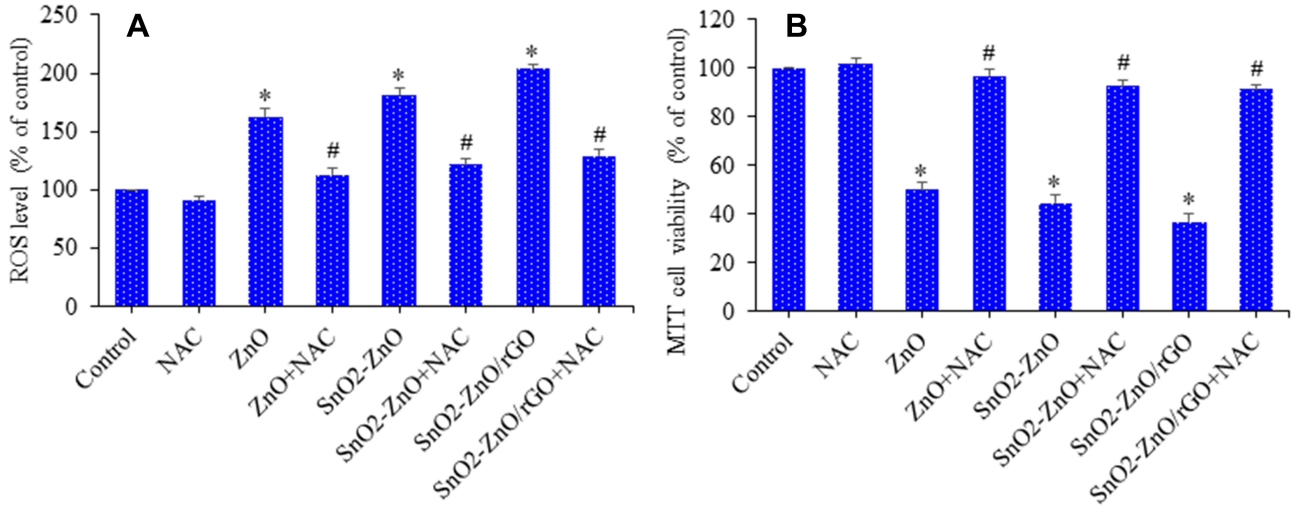

Figure 11 ROS mediated cytotoxicity. Cells were exposed for 24 h to 50 µg/mL of ZnO NPs, SnO_2-ZnO NPs, and SnO_2-ZnO/rGO NCs in the presence or absence of NAC. (**A**) ROS level with or without NAC. (**B**) Cell viability with or without NAC. Data represented as mean ±SD of five independent experiments (n=5). *Significantly different from the control (p<0.05). #Significantly different from ZnO NPs, SnO_2-ZnO NPs, and SnO_2-ZnO/rGO NCs groups (p<0.05).

NPs.[59,60] Hence, in this study, we further examined the role of ROS and oxidative stress in anticancer activity of SnO_2-ZnO/rGO NCs in MCF-7 cancer cells. Cells were exposed for 24 h to 50 µg/mL of ZnO NPs, SnO_2-ZnO NPs, and SnO_2-ZnO/rGO NCs in the presence and absence of NAC. Figure 11A demonstrated that NAC significantly alleviated the ROS generation induced by ZnO NPs, SnO_2-ZnO NPs, and SnO_2-ZnO/rGO NCs. We further found that NAC, efficiently reverted that cytotoxicity induced by ZnO NPs, SnO_2-ZnO NPs, and SnO_2-ZnO/rGO NCs (Figure 11B). These results confirm that SnO_2-ZnO/rGO NCs induced cytotoxicity in MCF-7 cancer cells was mediated through ROS generation. Altogether, our data suggested that SnO_2-ZnO/rGO NCs-induced toxicity in MCF-7 cells might be caused by ROS generation via mitochondrial pathway.

Effect of ZnO NPs, SnO_2-ZnO NPs, and SnO_2-ZnO/rGO NCs on Normal Human Mammary Epithelial (MCF10A) Cells

It is very important for anticancer drugs to have minimum or no effects on noncancerous normal cells. Benign nature of ZnO NPs against noncancerous normal cells have been reported previously.[11,14,61] Hence, at the end of this study, we examined the effects of ZnO NPs, SnO_2-ZnO NPs, and

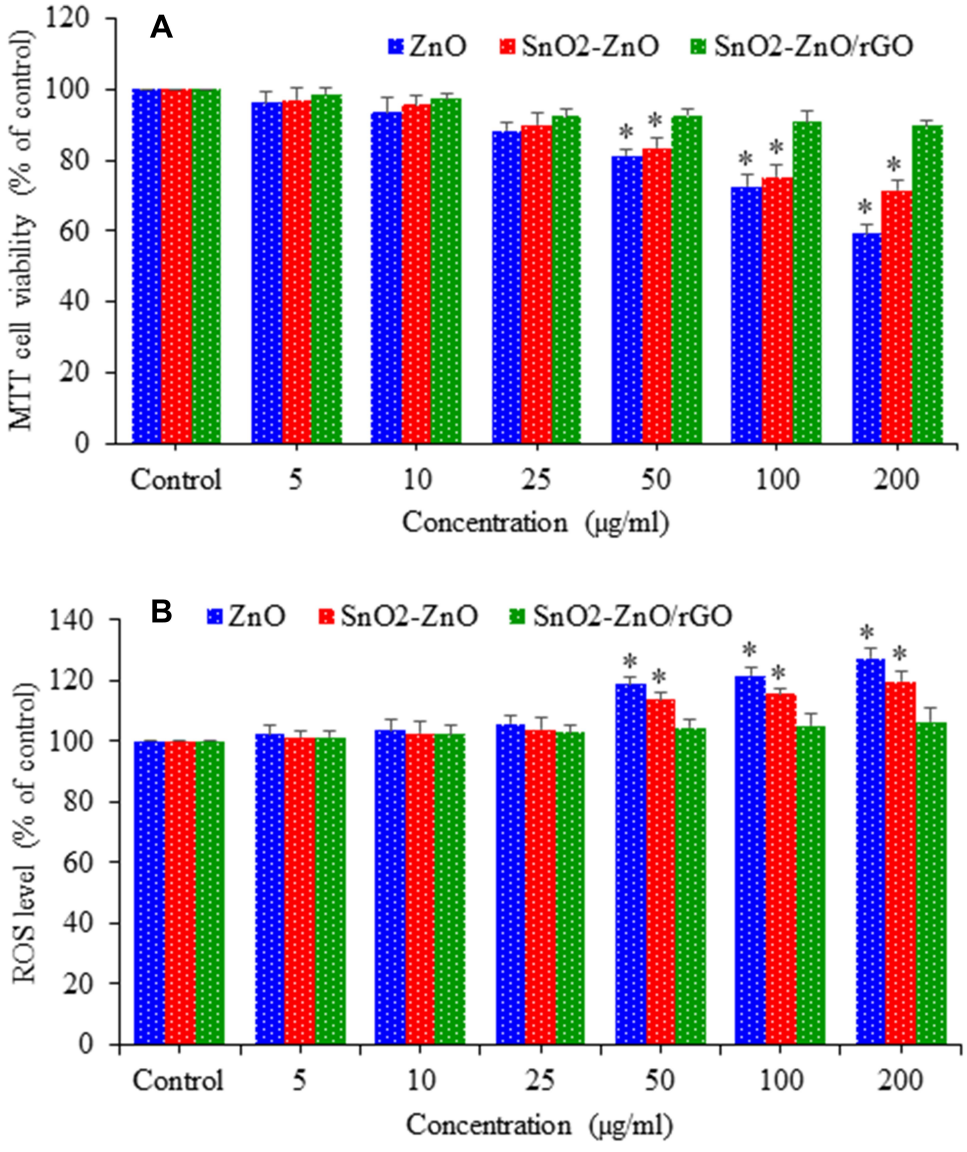

Figure 12 Effect of ZnO NPs, SnO_2-ZnO NPs, and SnO_2-ZnO/rGO NCs on normal human mammary epithelial (MCF10A) cells. Cells were treated for 24 h to different concentration of these samples (0–200 µg/mL), and cell viability and ROS level were determined. (**A**) MTT cell viability assay and (**B**) intracellular ROS level. Data represented as mean ±SD of five independent experiments (n=5). *Significantly different from the control ($p<0.05$).

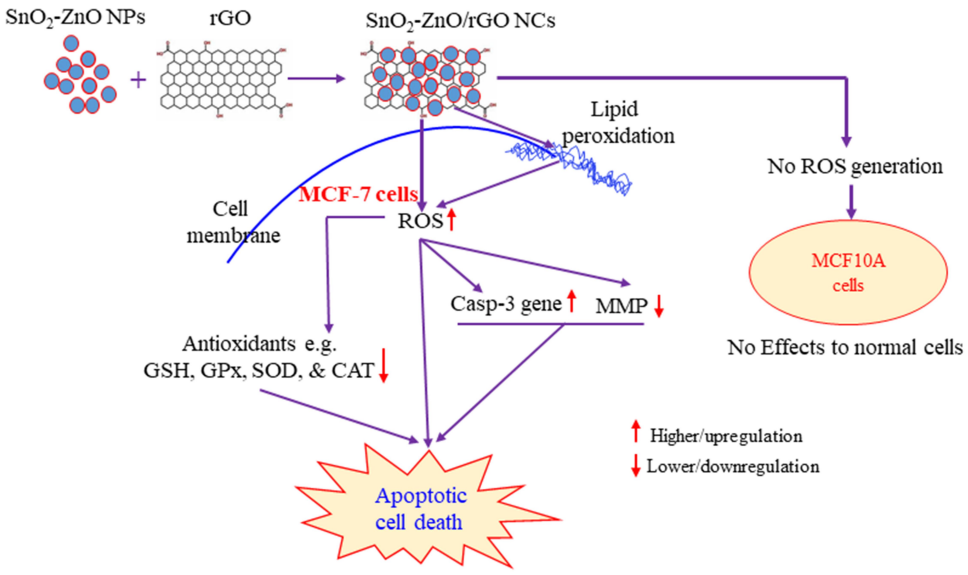

Figure 13 Possible mechanism of anticancer activity of SnO2-ZnO/rGO NCs.

SnO_2-ZnO/rGO NCs in normal breast cells (MCF10A). Cells were exposed to different concentrations (0–200 µg/mL) of these samples for 24 h. Figure 12A showed that ZnO NPs were not toxic to normal MCF10A cells up to 25 µg/mL concentration. However, cytotoxicity of pure ZnO NPs increases with increasing the concentrations from 50–200 µg/mL. In contrast, SnO_2-ZnO/rGO NCs were not toxic to normal MCF10A cells even at a higher concentration (200 µg/mL). These results suggested that in comparison to ZnO NPs and SnO_2-ZnO NPs, SnO_2-ZnO /rGO NCs have greater biocompatibility toward normal cells and higher cytotoxicity toward cancer cells. As we observed that ROS generation due to SnO_2-ZnO/rGO NCs exposure was the primary cause of killing of MCF-7 cancer cells. Hence, we further examined the ROS-generating potential of ZnO NPs, SnO_2-ZnO NPs, and SnO_2-ZnO/rGO NCs in MCF10A cells. As we can see that SnO_2-ZnO/rGO NCs did not induce intracellular ROS generation in normal human mammary epithelial cells even at 200 µg/mL (Figure 12B). Consequently, SnO_2-ZnO/rGO NCs showed improved anticancer activity and better biocompatibility compared to pure ZnO NPs. Possible mechanism of anticancer potential of SnO_2-ZnO/rGO NCs is presented as a schematic diagram (Figure 13).

Conclusion

In summary, SnO_2-ZnO/rGO NCs were successfully synthesized by a simple hydrothermal procedure. XRD data confirmed the formation of single-phase of hexagonal wurtzite ZnO. HRTEM and SEM mapping showed homogenous distribution of SnO_2 and rGO in ZnO NPs with high quality lattice fringes without any distortion. Band gap energy of SnO_2-ZnO/rGO NCs decreases after SnO_2 doping and rGO integration. The SnO_2-ZnO/rGO NCs demonstrated strong anticancer activity against MCF-7 cells compared to pure ZnO NPs. The SnO_2-ZnO/rGO NCs induced apoptosis in MCF-7 cancer cells through the upregulation of the caspase-3 gene and depletion of MMP. Mechanistic approach showed that SnO_2-ZnO/rGO NCs kill breast cancer cells through ROS generation via mitochondrial pathway. Moreover, biocompatibility of SnO_2-ZnO /rGO NCs was also greater in normal breast epithelia MCF10A cells than those of pure ZnO NPs. Overall our results provided a new approach to improve the selectivity and anticancer activity of ZnO in human breast cancer cells by tailoring its physicochemical properties. This work warrants further research on anti-tumor activity of SnO_2-ZnO/rGO NCs in animal breast cancer models.

Acknowledgments

This work was supported by the National Plan for Science, Technology, and Innovation (MAARIFAH), King Abdulaziz City for Science and Technology, Kingdom of Saudi Arabia, under Award 13-NAN908-02.

Author's Contribution

All authors made substantial contributions to conception and design, acquisition of data, or analysis and interpretation of data; took part in drafting the article or revising it critically for important intellectual content; agreed to submit to the current journal; gave final approval of the version to be published; and agree to be accountable for all aspects of the work.

Disclosure

The authors report no conflicts of interest in this work.

References

1. Wiesmann N, Tremel W, Brieger J. Zinc oxide nanoparticles for therapeutic purposes in cancer medicine. *J Mater Chem B*. 2020;8(23):4973–4989. doi:10.1039/d0tb00739k
2. Bray F, Ferlay J, Soerjomataram I, Siegel RL, Torre LA, Jemal A. Global cancer statistics 2018: GLOBOCAN estimates of incidence and mortality worldwide for 36 cancers in 185 countries. *CA Cancer J Clin*. 2018;68(6):394–424. doi:10.3322/caac.21492
3. Rasmussen JW, Martinez E, Louka P, Wingett DG. Zinc oxide nanoparticles for selective destruction of tumor cells and potential for drug delivery applications. *Expert Opin Drug Deliv*. 2010;7(9):1063–1077. doi:10.1517/17425247.2010.502560
4. Wicki A, Witzigmann D, Balasubramanian V, Huwyler J. Nanomedicine in cancer therapy: challenges, opportunities, and clinical applications. *J Controlled Release*. 2015;200:138–157. doi:10.1016/j.jconrel.2014.12.030
5. Ahamed M, Akhtar MJ, Majeed Khan MA, Alhadlaq HA. Oxidative stress mediated cytotoxicity of tin (IV) oxide (SnO2) nanoparticles in human breast cancer (MCF-7) cells. *Coll Surf B Biointerfaces*. 2018;172:152–160. doi:10.1016/j.colsurfb.2018.08.040
6. Akhtar MJ, Alhadlaq HA, Kumar S, Alrokayan SA, Ahamed M. Selective cancer-killing ability of metal-based nanoparticles: implications for cancer therapy. *Arch Toxicol*. 2015;89:11. doi:10.1007/s00204-015-1570-1
7. Ahamed M, Alhadlaq HA, Khan MAM, Akhtar MJ. Selective killing of cancer cells by iron oxide nanoparticles mediated through reactive oxygen species via p53 pathway. *J Nanoparticle Res*. 2013;15:1. doi:10.1007/s11051-012-1225-6
8. Ahamed M, Khan MAM, Akhtar MJ, Alhadlaq HA, Alshamsan A. Ag-doping regulates the cytotoxicity of TiO2 nanoparticles via oxidative stress in human cancer cells. *Sci Rep*. 2017;7(1):1–14. doi:10.1038/s41598-017-17559-9
9. Akhtar MJ, Ahamed M, Kumar S, Majeed Khan MA, Ahmad J, Alrokayan SA. Zinc oxide nanoparticles selectively induce apoptosis in human cancer cells through reactive oxygen species. *Int J Nanomedicine*. 2012;7. doi:10.2147/IJN.S29129
10. Tanino R, Amano Y, Tong X, et al. Anticancer activity of ZnO nanoparticles against human small-cell lung cancer in an orthotopic mouse model. *Mol Cancer Ther*. 2020;19(2):502–512. doi:10.1158/1535-7163.MCT-19-0018
11. Premanathan M, Karthikeyan K, Jeyasubramanian K, Manivannan G. Selective toxicity of ZnO nanoparticles toward Gram-positive bacteria and cancer cells by apoptosis through lipid peroxidation. *Nanomedicine*. 2011;7(2):184–192. doi:10.1016/j.nano.2010.10.001
12. Ahamed M, Akhtar MJ, Raja M, et al. ZnO nanorod-induced apoptosis in human alveolar adenocarcinoma cells via p53, survivin and bax/bcl-2 pathways: role of oxidative stress. *Nanomedicine*. 2011;7:6. doi:10.1016/j.nano.2011.04.011
13. Perera WPTD, Dissanayake RK, Ranatunga UI, et al. Curcumin loaded zinc oxide nanoparticles for activity-enhanced antibacterial and anticancer applications. *RSC Adv*. 2020;10(51):30785–30795. doi:10.1039/d0ra05755j
14. Akhtar MJ, Alhadlaq HA, Alshamsan A, Majeed Khan MA, Ahamed M. Aluminum doping tunes band gap energy level as well as oxidative stress-mediated cytotoxicity of ZnO nanoparticles in MCF-7 cells. *Sci Rep*. 2015;5. doi:10.1038/srep13876
15. Majeed Khan MA, Siwach R, Kumar S, Ahmed M, Ahmed J. Investigations on microstructure, optical, magnetic, photocatalytic, and dielectric behaviours of pure and Co-doped ZnO NPs. *J Mater Sci*. 2020;31(8):6360–6371. doi:10.1007/s10854-020-03192-2
16. Wang D, Li H, Liu Z, Zhou J, Zhang T. Acute toxicological effects of zinc oxide nanoparticles in mice after intratracheal instillation. *Int J Occup Environ Health*. 2017;23(1):11–19. doi:10.1080/10773525.2016.1278510
17. Verma SK, Panda PK, Jha E, Suar M, Parashar SKS. Altered physiochemical properties in industrially synthesized ZnO nanoparticles regulate oxidative stress; Induce in vivo cytotoxicity in embryonic zebrafish by apoptosis. *Sci Rep*. 2017;7(1):1. doi:10.1038/s41598-017-14039-y
18. Zhang W, Bao S, Fang T. The neglected nano-specific toxicity of ZnO nanoparticles in the yeast Saccharomyces cerevisiae. *Sci Rep*. 2016;6(1):1–11. doi:10.1038/srep24839
19. Franklin NM, Rogers NJ, Apte SC, Batley GE, Gadd GE, Casey PS. Comparative toxicity of nanoparticulate ZnO, bulk ZnO, and ZnCl2 to a freshwater microalga (Pseudokirchneriella subcapitata): the importance of particle solubility. *Environ Sci Technol*. 2007;41(24):8484–8490. doi:10.1021/es071445r
20. Mortimer M, Kasemets K, Kahru A. Toxicity of ZnO and CuO nanoparticles to ciliated protozoa Tetrahymena thermophila. *Toxicology*. 2010;269(2–3):182–189. doi:10.1016/j.tox.2009.07.007
21. Mishra PK, Mishra H, Ekielski A, Talegaonkar S, Vaidya B. Zinc oxide nanoparticles: a promising nanomaterial for biomedical applications. *Drug Discov Today*. 2017;22(12):1825–1834. doi:10.1016/j.drudis.2017.08.006
22. Ahamed M, Akhtar MJ, Khan MAM, Alaizeri ZM, Alhadlaq HA. Evaluation of the Cytotoxicity and Oxidative Stress Response of CeO2-RGO Nanocomposites in Human Lung Epithelial A549 Cells. *Nanomaterials*. 2019;9(12):1709. doi:10.3390/nano9121709
23. Wang J, Liu S, Cao X, et al. One-pot synthesis and gas sensitivity of SnO2 nanoparticles prepared using two Sn salts of SnCl4·5H2O and SnCl2·2H2O. *Appl Phys a Mater Sci Process*. 2020;126(1):44. doi:10.1007/s00339-019-3230-4
24. Khan MAM, Khan W, Ahamed M, Alhazaa AN. Investigation on the structure and physical properties of Fe 3 O 4/RGO nanocomposites and their photocatalytic application. *Mater Sci Semiconductor Proc*. 2019;99:44–53. doi:10.1016/j.mssp.2019.04.005
25. Yu H, Zhang B, Bulin C, Li R, High-efficient XR. Synthesis of Graphene Oxide Based on Improved Hummers Method. *Sci Rep*. 2016;6. doi:10.1038/srep36143
26. Mosmann T. Rapid colorimetric assay for cellular growth and survival: application to proliferation and cytotoxicity assays. *J Immunol Methods*. 1983;65(1–2):55–63. doi:10.1016/0022-1759(83)90303-4
27. Borenfreund E, Puerner JA. A simple quantitative procedure using monolayer cultures for cytotoxicity assays (HTD/NR-90). *J Tissue Culture Methods*. 1985;9(1):7–9. doi:10.1007/BF01666038
28. Ahamed M, Akhtar MJ, Siddiqui MA, et al. Oxidative stress mediated apoptosis induced by nickel ferrite nanoparticles in cultured A549 cells. *Toxicology*. 2011;283(2–3):101–108. doi:10.1016/j.tox.2011.02.010
29. Mohammad A, Saini RV, Kumar R, et al. A curious case of cysteines in human peroxiredoxin I. *Redox Biol*. 2020;37:101738. doi:10.1016/j.redox.2020.101738
30. Siddiqui MA, Alhadlaq HA, Ahmad J, Al-Khedhairy AA, Musarrat J, Ahamed M. Copper Oxide Nanoparticles Induced Mitochondria Mediated Apoptosis in Human Hepatocarcinoma Cells. *PLoS One*. 2013;8(8):8. doi:10.1371/journal.pone.0069534

31. Ellman GL. Tissue sulfhydryl groups. *Arch Biochem Biophys*. 1959;82(1):70–77. doi:10.1016/0003-9861(59)90090-6
32. Ohkawa H, Ohishi N, Yagi K. Assay for lipid peroxides in animal tissues by thiobarbituric acid reaction. *Anal Biochem*. 1979;95 (2):351–358. doi:10.1016/0003-2697(79)90738-3
33. Rotruck JT, Pope AL, Ganther HE, Swanson AB, Hafeman DG, Hoekstra WG. Selenium: biochemical role as a component of glatathione peroxidase. *Science*. 1973;179(4073):588–590. doi:10.1126/science.179.4073.588
34. Sinha AK. Colorimetric assay of catalase. *Anal Biochem*. 1972;47 (2):389–394. doi:10.1016/0003-2697(72)90132-7
35. Bradford MM. A rapid and sensitive method for the quantitation of microgram quantities of protein utilizing the principle of protein-dye binding. *Anal Biochem*. 1976;72(1–2):248–254. doi:10.1016/0003-2697(76)90527-3
36. Khan MAM, Kumar S, Alhazaa AN, Al-Gawati MA. Modifications in structural, morphological, optical and photocatalytic properties of ZnO:Mn nanoparticles by sol-gel protocol. *Mater Sci Semiconductor Proc*. 2018;87:134–141. doi:10.1016/j.mssp.2018.07.016
37. Faisal M, Ibrahim AA, Harraz FA, Bouzid H, Al-Assiri MS, Ismail AA. SnO2 doped ZnO nanostructures for highly efficient photocatalyst. *J Mol Catal a Chem*. 2015;397:19–25. doi:10.1016/j.molcata.2014.10.027
38. Zhu S, Fan L, Lu Y. Highly uniform Fe3O4 nanoparticle-rGO composites as anode materials for high performance lithium-ion batteries. *RSC Adv*. 2017;7(87):59939–59946. doi:10.1039/c7ra11779e
39. Hamrouni A, Moussa N, Parrino F, Di Paola A, Houas A, Palmisano L. Sol-gel synthesis and photocatalytic activity of ZnO-SnO2 nanocomposites. *J Mol Catal a Chem*. 2014;390:133–141. doi:10.1016/j.molcata.2014.03.018
40. Dargahi Z, Asgharzadeh H, Maleki-Ghaleh H. Synthesis of Mo-doped TiO2/reduced graphene oxide nanocomposite for photoelectrocatalytic applications. *Ceramics Int*. 2018;44(11):13015–13023. doi:10.1016/j.ceramint.2018.04.120
41. Khan MAM, Kumar S, Ahamad T, Alhazaa AN. Enhancement of photocatalytic and electrochemical properties of hydrothermally synthesized WO3 nanoparticles via Ag loading. *J Alloys Compd*. 2018;743:485–493. doi:10.1016/j.jallcom.2018.01.343
42. Zhang H, Pokhrel S, Ji Z, et al. PdO Doping Tunes Band-Gap Energy Levels as Well as Oxidative Stress Responses to a Co 3 O 4 p -Type Semiconductor in Cells and the Lung. *J Am Chem Soc*. 2014;136 (17):6406–6420. doi:10.1021/ja501699e
43. Mittal S, Kumar V, Dhiman N, Chauhan LKS, Pasricha R, Pandey AK. Physico-chemical properties based differential toxicity of graphene oxide/reduced graphene oxide in human lung cells mediated through oxidative stress. *Sci Rep*. 2016;6. doi:10.1038/srep39548
44. Ahamed M, Akhtar MJ, Alhadlaq HA. Influence of silica nanoparticles on cadmium-induced cytotoxicity, oxidative stress, and apoptosis in human liver HepG2 cells. *Environ Toxicol*. 2020;22895. doi:10.1002/tox.22895
45. Jiang J, Oberdörster G, Biswas P. Characterization of size, surface charge, and agglomeration state of nanoparticle dispersions for toxicological studies. *J Nanoparticle Res*. 2009;11(1):77–89. doi:10.1007/s11051-008-9446-4
46. Wang J, Lee JS, Kim D, Zhu L. Exploration of Zinc Oxide Nanoparticles as a Multitarget and Multifunctional Anticancer Nanomedicine. *ACS Appl Mater Interfaces*. 2017;9(46):39971–39984. doi:10.1021/acsami.7b11219
47. Khorsandi L, Farasat M. Zinc oxide nanoparticles enhance expression of maspin in human breast cancer cells. *Environ Sci Pollution Res*. 2020;27(30):38300–38310. doi:10.1007/s11356-020-09986-5
48. Zhang T, Du E, Liu Y, et al. Anticancer Effects of Zinc Oxide Nanoparticles Through Altering the Methylation Status of Histone on Bladder Cancer Cells. *Int J Nanomedicine*. 2020;15:1457–1468. doi:10.2147/IJN.S228839
49. Zhuang C, She Y, Zhang H, et al. Cytoprotective effect of deferiprone against aluminum chloride-induced oxidative stress and apoptosis in lymphocytes. *Toxicol Lett*. 2018;285:132–138. doi:10.1016/j.toxlet.2018.01.007
50. Balakireva AV, Zamyatnin AA. Cutting Out the Gaps Between Proteases and Programmed Cell Death. *Front Plant Sci*. 2019;10. doi:10.3389/fpls.2019.00704
51. Chang SY, Lee MY, Chung PS, et al. Enhanced mitochondrial membrane potential and ATP synthesis by photobiomodulation increases viability of the auditory cell line after gentamicin-induced intrinsic apoptosis. *Sci Rep*. 2019;9:1. doi:10.1038/s41598-019-55711-9
52. Duan X, Liao Y, Liu T, et al. Zinc oxide nanoparticles synthesized from Cardiospermum halicacabum and its anticancer activity in human melanoma cells (A375) through the modulation of apoptosis pathway. *J Photochem Photobiol B*. 2020;202:111718. doi:10.1016/j.jphotobiol.2019.111718
53. Wang S-W, Lee C-H, Lin M-S, et al. ZnO Nanoparticles Induced Caspase-Dependent Apoptosis in Gingival Squamous Cell Carcinoma through Mitochondrial Dysfunction and p70S6K Signaling Pathway. *Int J Mol Sci*. 2020;21(5):1612. doi:10.3390/ijms21051612
54. Perillo B, Di Donato M, Pezone A, et al. ROS in cancer therapy: the bright side of the moon. *Exp Mol Med*. 2020;52(2):192–203. doi:10.1038/s12276-020-0384-2
55. Yang Y, Song Z, Wu W, Xu A, Lv S, Ji S. ZnO Quantum Dots Induced Oxidative Stress and Apoptosis in HeLa and HEK-293T Cell Lines. *Front Pharmacol*. 2020;11. doi:10.3389/fphar.2020.00131
56. Akhtar MJ, Ahamed M, Alhadlaq HA, Alshamsan A. Mechanism of ROS scavenging and antioxidant signalling by redox metallic and fullerene nanomaterials: potential implications in ROS associated degenerative disorders. *Biochimica et Biophysica Acta*. 2017;1861:4. doi:10.1016/j.bbagen.2017.01.018
57. Kuang F, Liu J, Tang D, Oxidative Damage KR. Antioxidant Defense in Ferroptosis. *Front Cell Dev Biology*. 2020;8:969. doi:10.3389/fcell.2020.586578
58. Hasanuzzaman M, Bhuyan MHMB, Zulfiqar F, et al. Reactive oxygen species and antioxidant defense in plants under abiotic stress: revisiting the crucial role of a universal defense regulator. *Antioxidants*. 2020;9(8):1–52. doi:10.3390/antiox9080681
59. Sivakumar P, Lee M, Kim YS, Shim MS. Photo-triggered antibacterial and anticancer activities of zinc oxide nanoparticles. *J Mater Chem B*. 2018;6(30):4852–4871. doi:10.1039/c8tb00948a
60. Bai DP, Zhang XF, Zhang GL, Huang YF, Gurunathan S. Zinc oxide nanoparticles induce apoptosis and autophagy in human ovarian cancer cells. *Int J Nanomedicine*. 2017;12:6521–6535. doi:10.2147/IJN.S140071
61. Ostrovsky S, Kazimirsky G, Gedanken A, Brodie C. Selective cytotoxic effect of ZnO nanoparticles on glioma cells. *Nano Res*. 2009;2 (11):882–890. doi:10.1007/s12274-009-9089-5

International Journal of Nanomedicine Dovepress

Publish your work in this journal

The International Journal of Nanomedicine is an international, peer-reviewed journal focusing on the application of nanotechnology in diagnostics, therapeutics, and drug delivery systems throughout the biomedical field. This journal is indexed on PubMed Central, MedLine, CAS, SciSearch®, Current Contents®/Clinical Medicine, Journal Citation Reports/Science Edition, EMBase, Scopus and the Elsevier Bibliographic databases. The manuscript management system is completely online and includes a very quick and fair peer-review system, which is all easy to use. Visit http://www.dovepress.com/testimonials.php to read real quotes from published authors.

Submit your manuscript here: https://www.dovepress.com/international-journal-of-nanomedicine-journal